Modeling the kinematics of multi-axial composite laminates as a stacking of 2D TIF plies

Ruben Ibañez, Emmanuelle Abisset-Chavanne, Francisco Chinesta, and Antonio Huerta

Citation: AIP Conference Proceedings **1769**, 170046 (2016); doi: 10.1063/1.4963602
View online: http://dx.doi.org/10.1063/1.4963602
View Table of Contents: http://scitation.aip.org/content/aip/proceeding/aipcp/1769?ver=pdfcov
Published by the AIP Publishing

Modeling the kinematics of multi-axial composite laminates as a stacking of 2D TIF plies

Ruben Ibañez[1,b)], Emmanuelle Abisset-Chavanne[1,c)], Francisco Chinesta[1,a),d)] and Antonio Huerta[2,e)]

[1]*ICI Institute & ESI GROUP CHAIR, Centrale Nantes, 1 rue de la Noe, F-44300 Nantes, France.*
[2] *LaCaN, Universitat Politècnica de Catalunya, BarcelonaTech, 08034 Barcelona, Spain*

[a)]Corresponding author: Francisco.Chinesta@ec-nantes.fr
[b)]Ruben.Ibanez@ec-nantes.fr
[c)]Emmanuelle.Abisset-Chavanne@ec-nantes.fr
[d)]Francisco.Chinesta@ec-nantes.fr
[e)]antonio.huerta@upc.edu

Abstract. Thermoplastic composites are widely considered in structural parts. In this paper attention is paid to sheet forming of continuous fiber laminates. In the case of unidirectional prepregs, the ply constitutive equation is modeled as a transversally isotropic fluid, that must satisfy both the fiber inextensibility as well as the fluid incompressibility. When the stacking sequence involves plies with different orientations the kinematics of each ply during the laminate deformation varies significantly through the composite thickness. In our former works we considered two different approaches when simulating the squeeze flow induced by the laminate compression, the first based on a penalty formulation and the second one based on the use of Lagrange multipliers. In the present work we propose an alternative approach that consists in modeling each ply involved in the laminate as a transversally isotropic fluid – TIF - that becomes 2D as soon as incompressibility constraint and plane stress assumption are taken into account. Thus, composites laminates can be analyzed as a stacking of 2D TIF models that could eventually interact by using adequate friction laws at the inter-ply interfaces.

INTRODUCTION

Thermoplastic composites are preferred structural materials due to their excellent damage tolerance properties, shorter manufacturing cycles and ease of weldability. One of the precursor material to fabricate thermoplastic composite parts is an unidirectional (UD) prepreg which consists of aligned continuous fibers pre-impregnated with thermoplastic resin. In their melt state, UD prepreg can be viewed as inextensible fibers surrounded by an incompressible viscous matrix, and hence can be modeled as a transversally isotropic fluid – TIF –, also known as Ericksen fluid, [12]. These UD laminates are usually stacked in desired orientations to create a composite laminate.

The squeeze flow behaviour of both unidirectional and multiaxial laminates has been studied in our former work [9], where a penalty formulation of the Ericksen fluid flow using an appropriate in-plane-out-of-plane separated representation (widely considered in our former works [3, 5, 4, 6, 8]) wad employed.

In our former works we considered two different approaches when analyzing the squeeze flow induced by the laminate compression: (i) first a fully 3D penalty formulation and later (ii) a fully 3D mixed formulation in which both constraints (incompressibility and inextensibility) were introduced by using adequate Lagrange multipliers instead of using penalty coefficients. However both approaches seem computationally expensive and too intrusive from the point of view of their integration in commercial simulation codes. For those reasons in this paper we propose an alternative approach that consists in modeling each ply involved in the laminate as a transversally isotropic fluid – TIF - that becomes 2D as soon as incompressibility and plane stress are taken into account. Thus, composites laminates can be modeled as a 2D TIF model stacking that could eventually interact by using adequate friction laws at their interfaces

ESAFORM 2016
AIP Conf. Proc. 1769, 170046-1–170046-13; doi: 10.1063/1.4963602
Published by AIP Publishing. 978-0-7354-1427-3/$30.00

REVISITING TRANSVERSALLY ISOTROPIC FLUID MODELS

The TIF model

The Transversally Isotropic Fluid –TIF– also known as Ericksen fluid, is a viscous fluid complemented with a local inextensibility constraint along direction **p**. This model represents quite well the expected behavior of a unidirectional composite prepreg.

When considering the flow of a single ply represented by a TIF constitutive equation, the flow model is defined in the 3D plate domain Ξ whose plate-like geometry allows expressing it into the separated form $\Xi = \Omega \times \mathcal{I}$, with $\Omega \subset \mathbb{R}^2$ and $\mathcal{I} \subset \mathbb{R}$, that is no more than the tensor product of a 2D and 1D (related to the mould thickness) domains.

By defining the second order orientation tensor $\mathbf{a} = \mathbf{p} \otimes \mathbf{p}$ and assuming an inertia-free regime and an incompressible transversally isotropic fluid with director **p**, the flow model reads:

$$\left\{ \begin{array}{l} \nabla \cdot \boldsymbol{\sigma} = \mathbf{0} \\ \boldsymbol{\sigma} = -p\mathbf{I} + \tau \mathbf{a} + 2\eta_T \mathbf{D} + 2(\eta_L - \eta_T)(\mathbf{D} \cdot \mathbf{a} + \mathbf{a} \cdot \mathbf{D}) \\ \nabla \cdot \mathbf{v} = 0 \\ \mathbf{D} : \mathbf{a} = 0 \end{array} \right. , \tag{1}$$

where $\boldsymbol{\sigma}$ is the Cauchy's stress tensor, **I** the unit tensor, η_T the transversal fluid viscosity, η_L the longitudinal fluid viscosity, p the pressure (Lagrange multiplier associated with the incompressibility constraint), τ the fiber tension (Lagrange multiplier associated with the fiber inextensibility constraint) and the rate of strain tensor **D** defined as

$$\mathbf{D} = \frac{\nabla \mathbf{v} + (\nabla \mathbf{v})^T}{2}. \tag{2}$$

It the most general case, both Dirichlet and Neuman boundary conditions (BC) applied respectively in Γ_D and Γ_N:

$$\left\{ \begin{array}{ll} \mathbf{v} = \mathbf{v}_D & \text{in } \Gamma_D \\ \mathbf{t} = \boldsymbol{\sigma} \cdot \mathbf{n} & \text{in } \Gamma_N \end{array} \right. , \tag{3}$$

with $\Gamma_D \cup \Gamma_N = \Gamma \equiv \partial\Xi$ and $\Gamma_D \cup \Gamma_N = \emptyset$.

Flow model weak form

The problem weak form related to the flow model (1) results

$$\left\{ \begin{array}{l} \int_\Omega \mathbf{v}^* \cdot (\nabla \cdot \boldsymbol{\sigma}) = 0 \\ \int_\Omega p^* \, (\nabla \cdot \mathbf{v}) = 0 \\ \int_\Omega \tau^* \, (\mathbf{D} : \mathbf{a}) = 0 \end{array} \right. , \tag{4}$$

where $\mathbf{v}^*$, p^* and τ^* are the associated test functions defined in appropriate functional spaces for ensuring the usual stability conditions related to mixed formulations. In the previous equation the Cauchy stress is given by the TIF constitutive equation (second expression in (1) in which for the sake of simplicity and without loss of generality in the sequel it will assumed $\eta_L = \eta_T$) whose expression involves pressure, tension and velocity fields, p, τ and **v** respectively.

By integrating by parts the first equation in (4), and assuming as usually $\mathbf{v}^*(\mathbf{x} \in \Gamma_D) = \mathbf{0}$, it results:

$$\int_\Omega \mathbf{D}^* : \boldsymbol{\sigma} \, d\Omega = \int_\Gamma \mathbf{v}^* \cdot (\boldsymbol{\sigma} \cdot \mathbf{n}) \, d\Gamma = \int_{\Gamma_N} \mathbf{v}^* \cdot \mathbf{t} \, d\Gamma, \tag{5}$$

that introducing the TIF constitutive equation taking into account the simplifying hypothesis $\eta_L = \eta_T = \eta$, results

$$\int_\Omega 2\eta \, \mathbf{D}^* : \mathbf{D} \, d\Omega - \int_\Omega Tr(\mathbf{D}^*) \, p \, d\Omega + \int_\Omega \tau \mathbf{D}^* : \mathbf{a} \, d\Omega = \int_{\Gamma_N} \mathbf{v}^* \cdot \mathbf{t} \, d\Gamma. \tag{6}$$

When using stable functional approximations for interpolating velocity, pressure and tension fields respectively, e.g. Q2/P1/P1 as proved in our former works, the resulting discrete system reads:

$$\begin{bmatrix} \mathbf{K} & \mathbf{B}^T & \mathbf{C}^T \\ \mathbf{B} & \mathbf{0} & \mathbf{0} \\ \mathbf{C} & \mathbf{0} & \mathbf{0} \end{bmatrix} \begin{bmatrix} \mathbf{V} \\ \mathbf{P} \\ \mathbf{T} \end{bmatrix} = \begin{bmatrix} \mathbf{F} \\ \mathbf{0} \\ \mathbf{0} \end{bmatrix}, \tag{7}$$

where $\mathbf{V}$, $\mathbf{P}$ and $\mathbf{T}$ are the vectors containing the nodal velocities $\mathbf{v}$, pressures p and tensions τ. On the other hand $\mathbf{K}$ is the matrix that contains viscous contributions, $\mathbf{B}$ the one accounting for the flow incompressibility, $\mathbf{C}$ the one related to the inextensibility constraint and finally vector $\mathbf{F}$ contains the contribution of Neuman and Dirichlet boundary conditions.

Plane stress formulation

The transversally isotropic fluid constitutive model describing prepreg composite plies has been traditionally considered within the plane stress framework, that assumes null out-of-plane stress components, i.e.

$$\boldsymbol{\sigma}^{PS} = \begin{bmatrix} \sigma_{11} & \sigma_{12} & 0 \\ \sigma_{21} & \sigma_{22} & 0 \\ 0 & 0 & 0 \end{bmatrix}, \tag{8}$$

where the superscript $\bullet^{PS}$ refers to the consideration of the plane stress framework (this superscript will be omitted in the sequel for the sake of notational simplicity). The matrix form of the constitutive equation reads:

$$\begin{bmatrix} \sigma_{11} & \sigma_{12} & 0 \\ \sigma_{21} & \sigma_{22} & 0 \\ 0 & 0 & 0 \end{bmatrix} = -p \begin{bmatrix} 1 & 0 & 0 \\ 0 & 1 & 0 \\ 0 & 0 & 1 \end{bmatrix} + \tau \begin{bmatrix} a_{11} & a_{12} & 0 \\ a_{21} & a_{22} & 0 \\ 0 & 0 & 0 \end{bmatrix} + 2\eta \begin{bmatrix} D_{11} & D_{12} & D_{13} \\ D_{21} & D_{22} & D_{23} \\ D_{31} & D_{32} & D_{33} \end{bmatrix}, \tag{9}$$

where the symmetry conditions $\sigma_{ij} = \sigma_{ji}$ and $D_{ij} = D_{ji}$ apply, and where the local fiber orientation (defining the inextensibility director $\mathbf{p}$) was assumed plane, i.e. $\mathbf{p}^T = (p_x, p_y, 0)$.

The nullity of the out-of-plane components of the stress tensor implies:

$$p = 2\eta D_{33} = -2\eta(D_{11} + D_{22}), \tag{10}$$

where the incompressibility constraint $Tr(\mathbf{D}) = D_{11} + D_{22} + D_{33} = 0$ was taken into account. On the other hand we have $D_{13} = 0$ implying

$$\frac{\partial v_1}{\partial x_3} = -\frac{\partial v_3}{\partial x_1}, \tag{11}$$

and $D_{23} = 0$ that implies

$$\frac{\partial v_2}{\partial x_3} = -\frac{\partial v_3}{\partial x_2}. \tag{12}$$

Equation (10) allows expressing the pressure as a function of the in-plane components of the velocity. Therefore, the plane Cauchy stress tensor reads:

$$\begin{bmatrix} \sigma_{11} & \sigma_{12} \\ \sigma_{21} & \sigma_{22} \end{bmatrix} = \tau \begin{bmatrix} a_{11} & a_{12} \\ a_{21} & a_{22} \end{bmatrix} + 2\eta \begin{bmatrix} 2D_{11} + D_{22} & D_{12} \\ D_{21} & D_{11} + 2D_{22} \end{bmatrix}. \tag{13}$$

Thus, the associated weak form when considering plane stresses only involves the plane components of the velocity vector v_1 and v_2 as well as the scalar tension field τ. Thus the problem becomes 2D and it has the same structure than the one related to the standard Stokes problem, where moreover the mixed formulation stability condition (LBB) remains similar.

Thus, the final discrete system reduces to:

$$\begin{bmatrix} \tilde{\mathbf{K}} & \tilde{\mathbf{C}}^T \\ \tilde{\mathbf{C}} & \mathbf{0} \end{bmatrix} \begin{bmatrix} \tilde{\mathbf{V}} \\ \tilde{\mathbf{T}} \end{bmatrix} = \begin{bmatrix} \tilde{\mathbf{F}} \\ \mathbf{0} \end{bmatrix}, \tag{14}$$

where tildes are employed to indicate that this discrete system comes from the resulting 2D plane stress formulation involving 2 degrees of freedom at each velocity node and one at each node used for approximating the tension field.

2D TIF STACKING FOR DESCRIBING COMPOSITE LAMINATES

When considering a composite laminate the first option is modeling each ply using a plane-stress TIF model. In that case the ply will react to the applied loads (boundary conditions) deforming accordingly depending on the fiber orientation with respect to the applied loads. However, it is well kwon that a friction can appears at the plies interfaces where resin eventually lubricates the plies relative displacement.

The simplest viscous friction model consists of the Coulomb model that assumes a shear force that scales with the relative velocity between each two neighbor plies. It is easy to prove that such a friction coefficient η_f scales with the resin viscosity and the inverse of the lubrication layer thickness. In what follows we assume a linear dependence even if nonlinear frictions can be also easily considered.

In that case we consider planar surface forces due to the friction, acting in the plies having common interfaces. Thus, if interface i, $\mathcal{I}_i$, is located in between plies $\mathcal{P}_i$ and $\mathcal{P}_{i+1}$, the friction force at interface i, $\mathbf{f}_i^f$ given by

$$\mathbf{f}_i^f(\mathbf{x}) = \eta_f(\mathbf{v}_{i+1}(\mathbf{x}) - \mathbf{v}_i(\mathbf{x})), \tag{15}$$

will apply on both plies at position $\mathbf{x}$, having the same magnitude but opposite directions.

For illustrating the assembling procedure, we consider a three plies laminate, $\mathcal{P}_1$, $\mathcal{P}_2$ and $\mathcal{P}_3$, the first located at the bottom, the second one at the middle and the third one at the top. The discrete system writes:

$$\begin{bmatrix} \mathbf{K}_1 & \mathbf{C}_1^T & \mathbf{0} & \mathbf{0} & \mathbf{0} & \mathbf{0} \\ \mathbf{C}_1 & \mathbf{0} & \mathbf{0} & \mathbf{0} & \mathbf{0} & \mathbf{0} \\ \mathbf{0} & \mathbf{0} & \mathbf{K}_2 & \mathbf{C}_2^T & \mathbf{0} & \mathbf{0} \\ \mathbf{0} & \mathbf{0} & \mathbf{C}_2 & \mathbf{0} & \mathbf{0} & \mathbf{0} \\ \mathbf{0} & \mathbf{0} & \mathbf{0} & \mathbf{0} & \mathbf{K}_3 & \mathbf{C}_3^T \\ \mathbf{0} & \mathbf{0} & \mathbf{0} & \mathbf{0} & \mathbf{C}_3 & \mathbf{0} \end{bmatrix} \begin{bmatrix} \mathbf{V}_1 \\ \mathbf{T}_1 \\ \mathbf{V}_2 \\ \mathbf{T}_2 \\ \mathbf{V}_3 \\ \mathbf{T}_3 \end{bmatrix} = \begin{bmatrix} \mathbf{F}_1 + \mathbf{F}_1^f \\ \mathbf{0} \\ \mathbf{F}_2 + \mathbf{F}_2^f \\ \mathbf{0} \\ \mathbf{F}_3 + \mathbf{F}_3^f \\ \mathbf{0} \end{bmatrix}, \tag{16}$$

that expressing the dependence of the nodal friction forces on the relative nodal velocities, the previous system becomes

$$\begin{bmatrix} \mathbf{K}_1 + \mathbf{D}_1 & \mathbf{C}_1^T & -\mathbf{D}_1 & \mathbf{0} & \mathbf{0} & \mathbf{0} \\ \mathbf{C}_1 & \mathbf{0} & \mathbf{0} & \mathbf{0} & \mathbf{0} & \mathbf{0} \\ -\mathbf{D}_1 & \mathbf{0} & \mathbf{K}_2 + \mathbf{D}_1 + \mathbf{D}_2 & \mathbf{C}_2^T & -\mathbf{D}_2 & \mathbf{0} \\ \mathbf{0} & \mathbf{0} & \mathbf{C}_2 & \mathbf{0} & \mathbf{0} & \mathbf{0} \\ \mathbf{0} & \mathbf{0} & -\mathbf{D}_2 & \mathbf{0} & \mathbf{K}_3 + \mathbf{D}_2 & \mathbf{C}_3^T \\ \mathbf{0} & \mathbf{0} & \mathbf{0} & \mathbf{0} & \mathbf{C}_3 & \mathbf{0} \end{bmatrix} \begin{bmatrix} \mathbf{V}_1 \\ \mathbf{T}_1 \\ \mathbf{V}_2 \\ \mathbf{T}_2 \\ \mathbf{V}_3 \\ \mathbf{T}_3 \end{bmatrix} = \begin{bmatrix} \mathbf{F}_1 \\ \mathbf{0} \\ \mathbf{F}_2 \\ \mathbf{0} \\ \mathbf{F}_3 \\ \mathbf{0} \end{bmatrix}. \tag{17}$$

In the last expression matrices $\mathbf{D}_i$ are the same in the linear case as soon as lubrication layers have the same thickness. Obviously all these matrix vanish as soon as the friction coefficient η_f vanishes.

NUMERICAL RESULTS

The numerical results discussed hereafter consider several cases involving 3 plies, $\mathcal{P}_1$, $\mathcal{P}_2$ and $\mathcal{P}_3$. Different boundary conditions are applied related to traction or shear working conditions, considering different orientation directors at each ply.

The main aim of this section is to analyse the representation of a 3D composite laminate from a stacking of 2D plane-stress TIF plies interacting by means of friction forces.

Figure 1 depicts the laminate domain of length L and width W, with $\Omega = [0, L] \times [0, W]$. The four sides of Ω will be noted by W, E, N, and S, for the ones located respectively on the west (left), east (right), north (top) and south (bottom).

Inter-ply friction

Traction test

The three plies consist of uniaxial prepegs whose orientation directors align along 0/90/0 (in degrees). The W-side of the domain is clamped, that is $\mathbf{v}(x = 0, y) = \mathbf{0}$ and a positive traction $\mathbf{t} = (t, 0)^T$ plies on the E-side, with $t = 1$ (units

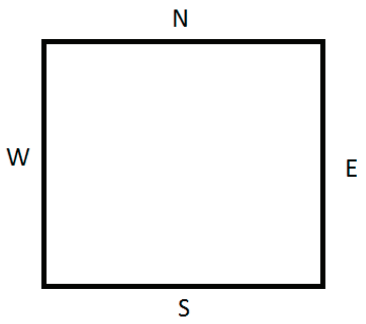

FIGURE 1. Laminate domain.

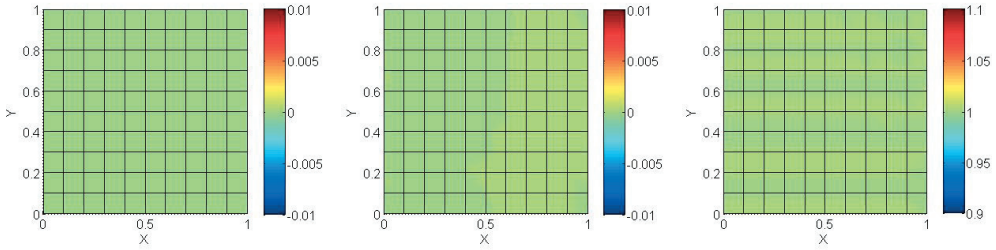

FIGURE 2. Traction applied on a laminate without friction forces. Ply $\mathcal{P}_1$: Horizontal velocity $u(\mathbf{x})$ (left); Vertical velocity $v(\mathbf{x})$ (center) and tension $\tau(\mathbf{x})$ (right).

in the metric system). On both, the N-side and the S-side, null tractions are applied. The longitudinal and transversal fluid viscosities are set to $10\text{Pa}\cdot\text{s}$, and when considering non-null friction $\eta_f = 0.1\text{Pa}\cdot\text{s}\cdot\text{m}^{-1}$.

Non-friction case

Solving the non-friction case is equivalent of solving the uncoupled case (each ply deforms independently of the neighbors plies).

Figure 2 depicts the velocity and the tension fields in ply $\mathcal{P}_1$ when friction forces are not considered. As it can be noticed the tension applied on the E-side is fully transmitted to the fibers whose tension corresponds to the applied traction, and the inextensibility results in zero velocities in both the horizontal and vertical directions.

Figure 3 depicts the corresponding fields in ply $\mathcal{P}_2$. In can be noticed that a non-zero velocity appears in the horizontal direction evolving almost linearly. In absence of fibers the ply would shortened in the vertical direction, but the fibers inextensibility avoid such a decrease in the width and for that fibers are subjected to a compressive tension.

Figure 4 depicts the associated results in ply $\mathcal{P}_3$ that as expected are exactly the same that those found in ply $\mathcal{P}_1$.

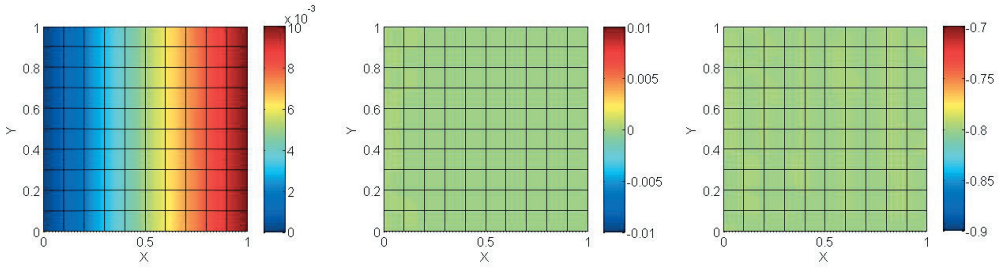

FIGURE 3. Traction applied on a laminate without friction forces. Ply $\mathcal{P}_2$: Horizontal velocity $u(\mathbf{x})$ (left); Vertical velocity $v(\mathbf{x})$ (center) and tension $\tau(\mathbf{x})$ (right).

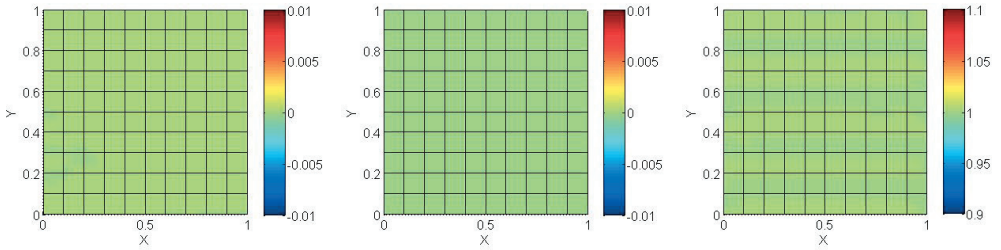

FIGURE 4. Traction applied on a laminate without friction forces. Ply $\mathcal{P}_3$: Horizontal velocity $u(\mathbf{x})$ (left); Vertical velocity $v(\mathbf{x})$ (center) and tension $\tau(\mathbf{x})$ (right).

Inter-ply friction

Figures 5, 6 and 7 depict similar results when considering inter-ply friction. In what concerns plies $\mathcal{P}_1$ and $\mathcal{P}_3$ as expected velocities vanish as was the case when neglecting friction, because their kinematics is controlled by the fiber inextensibility. However, in what concerns the tension, results are quite different. It is expected that a non-null horizontal velocity appears in ply $\mathcal{P}_2$ that will coincide with the relative velocity at both inter-plies interfaces. Thus a tension is transmitted from ply $\mathcal{P}_2$ to the top and bottom plies whose tension increases when moving from the E-side

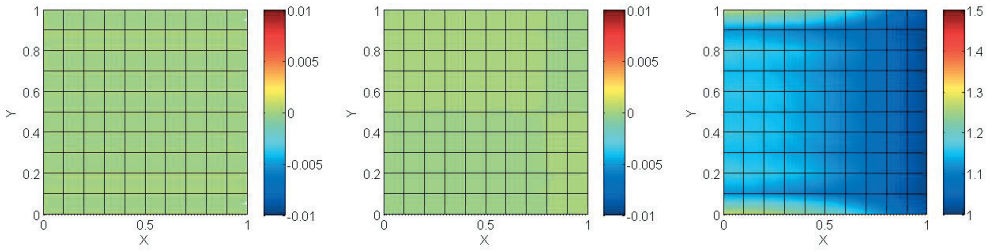

FIGURE 5. Traction applied on a laminate with inter-ply friction. Ply $\mathcal{P}_1$: Horizontal velocity $u(\mathbf{x})$ (left); Vertical velocity $v(\mathbf{x})$ (center) and tension $\tau(\mathbf{x})$ (right).

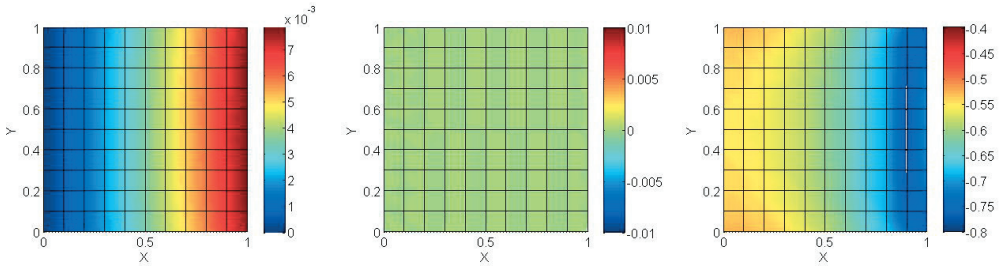

FIGURE 6. Traction applied on a laminate with inter-ply friction. Ply $\mathcal{P}_2$: Horizontal velocity $u(\mathbf{x})$ (left); Vertical velocity $v(\mathbf{x})$ (center) and tension $\tau(\mathbf{x})$ (right).

to the W-side. The tension on the W-sides of plies $\mathcal{P}_1$ and $\mathcal{P}_3$ must equilibrate the external applied traction and all the friction transmitted from the middle ply.

In what concerns the middle ply, because the friction the horizontal velocity remains almost linear but its magnitude is lower than when friction was not considered. For the same reason the compressive tension decreases.

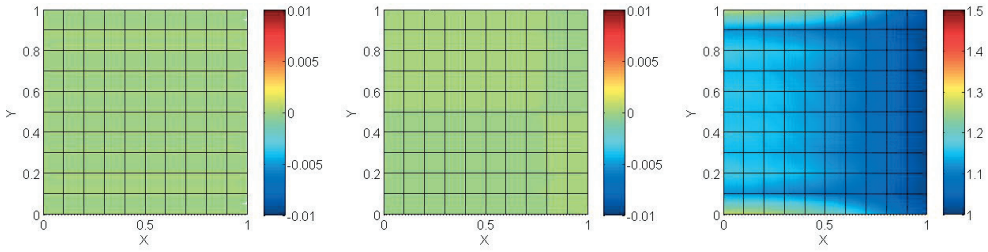

FIGURE 7. Traction applied on a laminate with inter-ply friction. Ply $\mathcal{P}_3$: Horizontal velocity $u(\mathbf{x})$ (left); Vertical velocity $v(\mathbf{x})$ (center) and tension $\tau(\mathbf{x})$ (right).

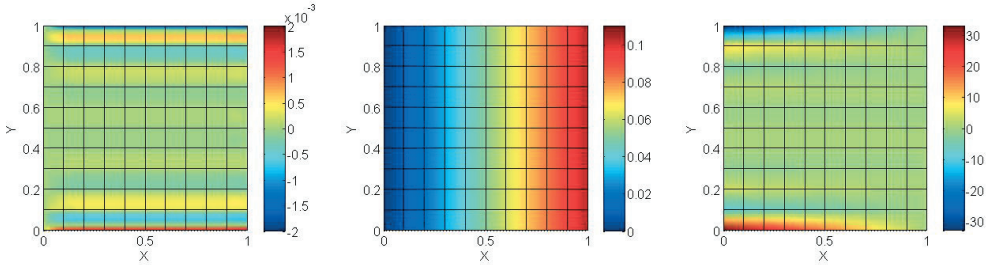

FIGURE 8. Shear applied on a laminate without friction forces. Ply $\mathcal{P}_1$: Horizontal velocity $u(\mathbf{x})$ (left); Vertical velocity $v(\mathbf{x})$ (center) and tension $\tau(\mathbf{x})$ (right).

Shear test

In this section we consider the same laminate and fluid parameters considered previously, but now the loading applying on the E-side consists of a shear stress $\mathbf{t} = (0, 1)^T$. Again the case of inter-ply friction is compared with its absence.

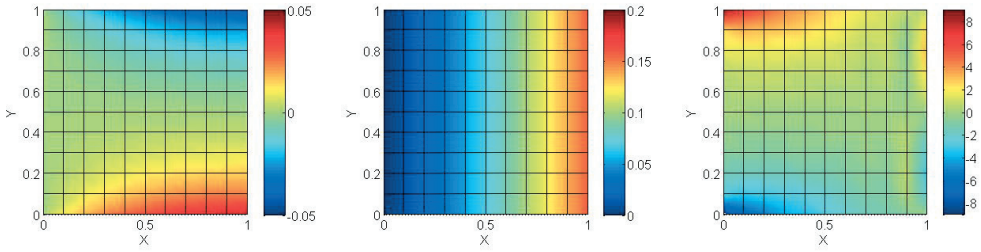

FIGURE 9. Shear applied on a laminate without friction forces. Ply $\mathcal{P}_2$: Horizontal velocity $u(\mathbf{x})$ (left); Vertical velocity $v(\mathbf{x})$ (center) and tension $\tau(\mathbf{x})$ (right).

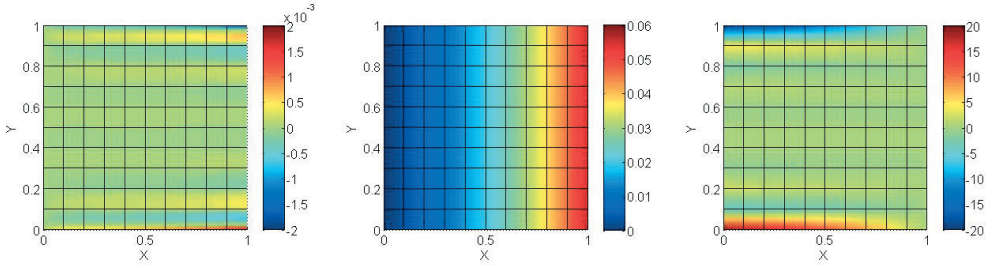

FIGURE 10. Shear applied on a laminate with inter-ply friction. Ply $\mathcal{P}_1$: Horizontal velocity $u(\mathbf{x})$ (left); Vertical velocity $v(\mathbf{x})$ (center) and tension $\tau(\mathbf{x})$ (right).

Non-friction case

Figures 8 and 9 depict velocities and tension in plies $\mathcal{P}_1$ and $\mathcal{P}_2$ respectively (again solution in $\mathcal{P}_3$ coincides with the one obtained in ply $\mathcal{P}_1$).

In ply $\mathcal{P}_1$, as expected, the horizontal velocity is almost null while the vertical velocity increases almost linearly when moving from the W-side to the E-side. The tension is almost zero everywhere, with fibers compressed in the top and extended at the bottom. As in classical beam theory and become the quasi-infinity fibers rigidity (related to the

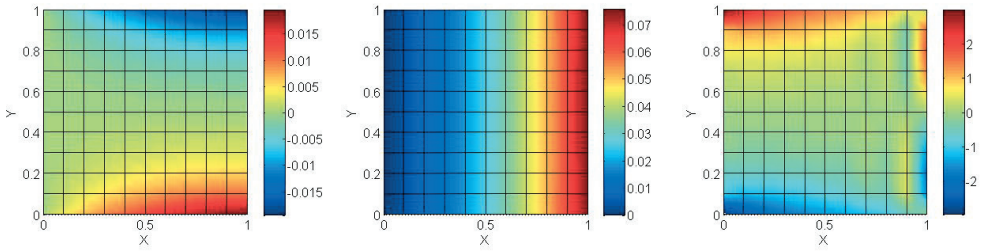

FIGURE 11. Shear applied on a laminate with inter-ply friction. Ply $\mathcal{P}_2$: Horizontal velocity $u(\mathbf{x})$ (left); Vertical velocity $v(\mathbf{x})$ (center) and tension $\tau(\mathbf{x})$ (right).

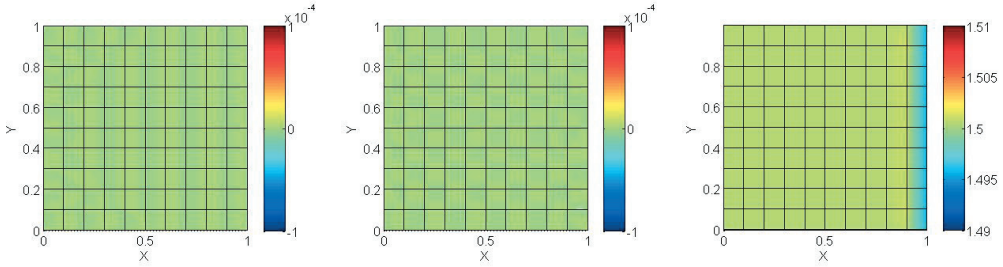

FIGURE 12. Traction applied on a laminate with very large inter-ply friction. Ply $\mathcal{P}_1$: Horizontal velocity $u(\mathbf{x})$ (left); Vertical velocity $v(\mathbf{x})$ (center) and tension $\tau(\mathbf{x})$ (right).

inextensibiliy) only fibers at the top and the bottom work.

Concerning ply $\mathcal{P}_2$, results are quite close to a priori expectations, with a horizontal velocity that approaches a rigid rotation on the E-side, a vertical velocity evolving almost linearly and fibers aligned in the vertical directions working in the clamped side neighborhood.

When considering inter-plies friction results are qualitatively very close to those obtained when ignoring inter-plies friction, however in the present case and as was the case when considering a traction loading the magnitude of the resulting velocities was again lower because friction tries to minimize the plies relative velocities, as shown in

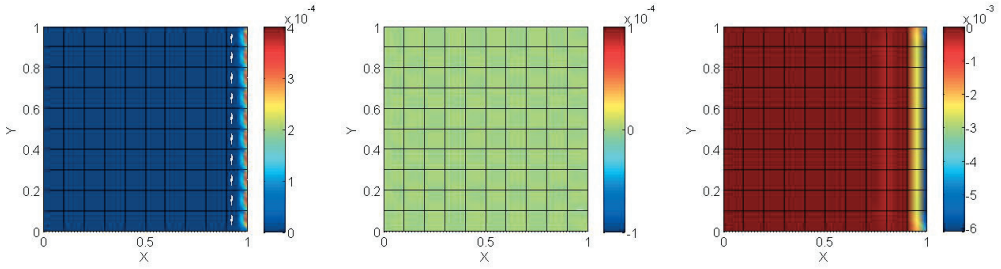

FIGURE 13. Traction applied on a laminate with very large inter-ply friction. Ply $\mathcal{P}_2$: Horizontal velocity $u(\mathbf{x})$ (left); Vertical velocity $v(\mathbf{x})$ (center) and tension $\tau(\mathbf{x})$ (right).

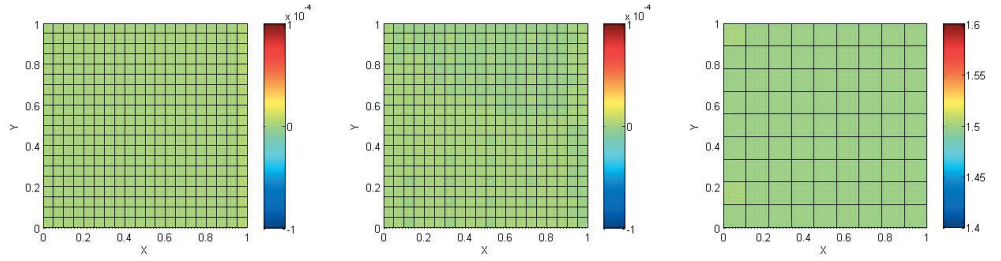

FIGURE 14. 3D finite element solution when traction is applied on a laminate. Ply $\mathcal{P}_1$: Horizontal velocity $u(\mathbf{x})$ (left); Vertical velocity $v(\mathbf{x})$ (center) and tension $\tau(\mathbf{x})$ (right).

Figs. 10 and 11. The same behavior applies for the tension field.

2D TIF model stacking versus fully 3D modeling

In this section we analyze the validity of models based of the 2D TIF model stacking with respect to fully 3D TIF models, when considering the same laminate that was addressed previously consisting of a unit traction applied of the E-side of the three plies laminate.

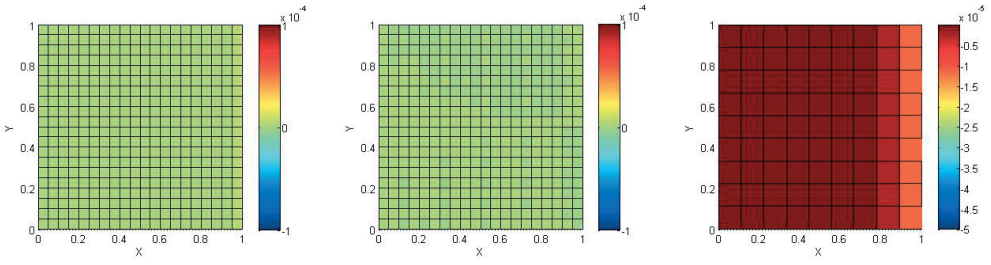

FIGURE 15. 3D finite element solution when traction is applied on a laminate. Ply $\mathcal{P}_2$: Horizontal velocity $u(\mathbf{x})$ (left); Vertical velocity $v(\mathbf{x})$ (center) and tension $\tau(\mathbf{x})$ (right).

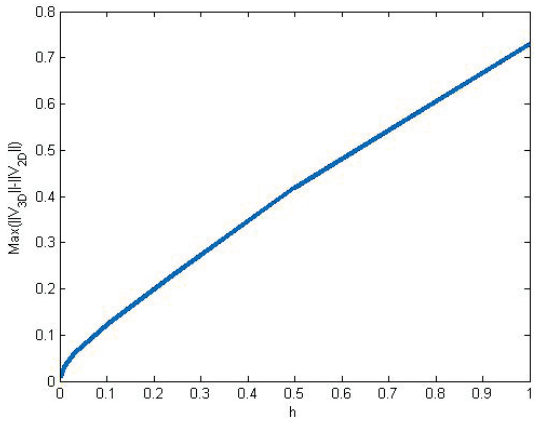

FIGURE 16. Error in the velocity norm when comparing the fully 3D solution with the one related to a 2D TIF model stacking

In the 3D case we consider the model described in section 2 that is discretized using a stable mixed finite element approximation $Q2/P1/P1$ assuming a continuos velocity approximation along the laminate thickness. This scenario is equivalent of considering the stacking of 2D TIF models with an infinite (in practice large enough) friction coefficient η_f.

First we check that in those circumstances, as soon as each ply in the fully 3D model consists of a single element, the 3D model should reduce to the 2D TIF stacking, where velocities are expected vanishing because the too constrained kinematics.

Figure 12 shows the resulting velocity and tension in the top and bottom plies when using the 2D TIF model stacking. As expected the velocity vanishes whereas the tension increases from 1 to 1.5 in order to take into account that the middle plain does not work (the friction coefficient is very large and fibers in the middle plane orients perpendicularly to the applied tension) as depicted in Fig. 13. The equilibrium is trivially satisfied: $2 \times 1.5 = 3 \times 1$.

Now, the same problem is solved using a fully 3D stable formulation. The solutions in plies $\mathcal{P}_1$ and $\mathcal{P}_2$ are

depicted respectively in Figs. 14 and 15, where almost the same results are found.

However, as soon as the ply is discretized by using several elements along the ply thickness the 3D solution is expected differing from the one related to the 2D TIF model stacking. This is due to the fact that in the middle ply, in which fibers are aligned orthogonally with respect to the direction of the applied traction, the TIF fluid can flow, generating an almost parabolic profile of the x-component of the velocity vector along the thickness of the middle ply. This behavior does not exist when considering the laminate as a sequence of 2D TIF plies with a large enough friction coefficient ensuring the velocity continuity along the laminate thickness. However, this deviation is expected decreasing with the plies thickness because the velocity should tends to zero all along the middle-ply thickness in order to avoid the divergence of the shear stresses at the plies interfaces. Thus, the norm of the error between the fully 3D and the 2D TIF stacking is expected decreasing with the plies thickness h. This expected behavior is confirmed in Fig. 16

Conclusions

A new numerical procedure is proposed to simulate the composite material sheet forming of multiaxial laminates. It is based on the modeling of the different laminate plies as a 2D plane-stress transversally isotropic fluid. These plies can deform independently when assuming no-friction at the inter-plies interfaces to adapt to the applied loads, or deforming in a coupled way when assuming a sort of friction at the plies interfaces, with the friction forces scaling with the relative velocity of the plies that meets at each interface.

It has been proved that such a modeling approche remains only valid (accurate enough) when the plis thickness remains small enough.

REFERENCES

[1] S. Aghighi, A. Ammar, C. Metivier, M. Normandin, F. Chinesta. Non incremental transient solution of the Rayleigh-Bénard convection model using the PGD. Journal of Non-Newtonian Fluid Mechanics, 200, 65-78, 2013.

[2] M.S. Aghighi, A. Ammar, C. Metivier, F. Chinesta. Parametric solution of the Rayleigh-Bénard convection model by using the PGD: Application to nanofluids. International Journal of Numerical Methods for Heat and Fluid Flows. In press.

[3] A. Ammar, B. Mokdad, F. Chinesta and R. Keunings, A new family of solvers for some classes of multi-dimensional partial differential equations encountered in kinetic theory modeling of complex fluids, J. Non-Newtonian Fluid Mech., 139, 153-176, 2006.

[4] B. Bognet, A. Leygue, F. Chinesta, A. Poitou and F. Bordeu, Advanced simulation of models defined in plate geometries: 3D solutions with 2D computational complexity, Computer Methods in Applied Mechanics and Engineering, 201, 1-12, 2012.

[5] F. Chinesta, A. Ammar, A. Leygue and R. Keunings, An overview of the Proper Generalized Decomposition with applications in computational rheology, J. Non-Newtonian Fluid Mech., 166, 578-592, 2011.

[6] F. Chinesta, A. Leygue, B. Bognet, Ch. Ghnatios, F. Poulhaon, F. Bordeu, A. Barasinski, A. Poitou, S. Chatel and S. Maison-Le-Poec, First steps towards an advanced simulation of composites manufacturing by automated tape placement, International Journal of Material Forming, http://www.springerlink.com/index/10.1007/s12289-012-1112-9

[7] J.L. Ericksen. Anisotropic Fluids. Archive for Rational Mechanics and Analysis, 231-237, 1959.

[8] Ch. Ghnatios, F. Chinesta, Ch. Binetruy. The Squeeze Flow of Composite Laminates. International Journal of Material Forming, 8, 73-83, 2015.

[9] Ch. Ghnatios, E. Abisset-Chavanne, Ch. Binetruy, F. Chinesta, S. Advani. 3D Modeling of Squeeze Flow of Multiaxial Laminates. Journal of Non-Newtonian Fluid Mechanics. Submitted.

[10] S.F. Shuler, S.G. Advani. Transverse squeeze flow of concentrated aligned fibers in viscous fluids. J. Non-Newtonian Fluid Mech., 65, 47-74, 1996.

[11] S.F. Shuler, S. Advani. Flow instabilities during the squeeze flow of multiaxial laminates. Journal of Composite Materials, 31/21, 2156-2160,1997.

[12] Spencer AJM, Theory of fabric-reinforced viscous fluids, Composites Part A, 2000, 31, 1311-1321.